Structural basis for the magnesium-dependent activation of transketolase from Chlamydomonas reinhardtii

(Article begins on next page)

20 April 2024

Rights / License:

Structural basis for the magnesium-dependent activation of transketolase from *Chlamydomonas reinhardtii*

Miriam Pasquini[a], Simona Fermani[b,*], Daniele Tedesco[a], Chiara Sciabolini[b], Pierre Crozet[c], Marina Naldi[a,d], Julien Henri[c], Ute Vothknecht[e], Carlo Bertucci[a], Stéphane D. Lemaire[c], Mirko Zaffagnini[a,*], Francesco Francia[a]

[a] Department of Pharmacy and Biotechnology, University of Bologna, Bologna, Italy

[b] Department of Chemistry "G. Ciamician", University of Bologna, Bologna, Italy

[c] Institut de Biologie Physico-Chimique, UMR8226, Laboratoire de Biologie Moléculaire et Cellulaire des Eucaryotes CNRS, Sorbonne Universités, UPMC Univ Paris 06, Paris, France.

[d] Center for Applied Biomedical Research, S. Orsola-Malpighi University Hospital, Bologna, Italy.

[e] Institute of Cellular and Molecular Botany, University of Bonn, Bonn, Germany

* Corresponding authors:

Mirko Zaffagnini,

Email: mirko.zaffagnini3@unibo.it;

Address: Via Irnerio 42, 40126, Bologna (BO), Italy

Telephone: +39-051-2091314

Simona Fermani,

Email: simona.fermani@unibo.it

Address: Via Selmi 2, 40126, Bologna (BO), Italy

Telephone: +39-051-2099475

Abstract

Background: In photosynthetic organisms, transketolase (TK) is involved in the Calvin-Benson cycle and participates to the regeneration of ribulose-5-phosphate. Previous studies demonstrated that TK catalysis is strictly dependent on thiamine pyrophosphate (TPP) and divalent ions such as Mg^{2+}.

Methods: TK from the unicellular green alga *Chlamydomonas reinhardtii* (CrTK) was recombinantly produced and purified to homogeneity. Biochemical properties of the CrTK enzyme were delineated by activity assays and its structural features determined by CD analysis and X-ray crystallography.

Results: CrTK is homodimeric and its catalysis depends on the reconstitution of the holo-enzyme in the presence of both TPP and Mg^{2+}. Activity measurements and CD analysis revealed that the formation of fully active holo-CrTK is Mg^{2+}-dependent and proceeds with a slow kinetics. The 3D-structure of CrTK without cofactors ($CrTK_{apo}$) shows that two portions of the active site are flexible and disordered while they adopt an ordered conformation in the holo-form. Oxidative treatments revealed that Mg^{2+} participates in the redox control of CrTK by changing its propensity to be inactivated by oxidation. Indeed, the activity of holo-form is unaffected by oxidation whereas CrTK in the apo-form or reconstituted with the sole TPP show a strong sensitivity to oxidative inactivation.

Conclusion: These evidences indicate that Mg^{2+} is fundamental to allow gradual conformational arrangements suited for optimal catalysis. Moreover, Mg^{2+} is involved in the control of redox sensitivity of CrTK.

General significance: The importance of Mg^{2+} in the functionality and redox sensitivity of CrTK is correlated to light-dependent fluctuations of Mg^{2+} in chloroplasts.

1. Introduction

Transketolase (TK) is a ubiquitous enzyme operating in the non-oxidative branch of the pentose phosphate pathway (PPP) and in the Calvin-Benson cycle (CBC) in photosynthetic organisms [1-4]. It catalyzes the transfer of a glycolaldehyde fragment from a ketose donor onto an aldose acceptor. D-xylulose-5-phosphate (X5P), fructose-6-phosphate (F6P) and sedoheptulose-7-phosphate (S7P) are typical donor substrates for TK, while glyceraldehyde-3-phosphate (G3P), D-ribose-5-phosphate (R5P) and D-erythrose-4-phosphate (E4P) are typical acceptor substrates [1,2]. Hence, within the CBC, TK catalyzes the conversion of fructose-6-phosphate/sedoheptulose-7-phosphate and glyceraldehyde-3-phosphate into erythrose-4-phosphate/ribose-5-phosphate and xylulose-5-phosphate, contributing to the regeneration of ribulose-5-phosphate [5]. All possible reactions are reversible and require the presence of both thiamine pyrophosphate (TPP) and divalent metal ions as TK cofactors. In the three-dimensional structure of TK from *Saccharomyces cerevisiae,* a Ca^{2+} ion is stabilized by TPP, the conserved residues Asp157, Asn187, and Ile189 and a water molecule [6,7]. Earlier studies on the same enzyme indicated that Ca^{2+}, Mg^{2+}, Mn^{2+}, Co^{2+} and Ni^{2+} can replace each other without affecting the maximal catalytic activity [8]. Although several three-dimensional structures from different sources have been solved, the chloroplastic TK from *Zea mays*, containing Mg^{2+} and TPP in the active site, is the only one belonging to a photosynthetic organism reported to date [9].

Several CBC enzymes (sedoheptulose-1,7-bisphosphatase, SBPase; phosphoribulokinase, PRK; glyceraldehyde-3-phosphate dehydrogenase, GAPDH; fructose-1,6-bisphosphatase, FBPase; and phosphoglycerate kinase, PGK) have a low activity in the dark and are activated in the light through reduction of regulatory disulfide bonds by the ferredoxin-thioredoxin system [10,11]. This system, composed of ferredoxin, ferredoxin-thioredoxin reductase (FTR) and thioredoxin (TRX), converts a photosynthetic signal received from photosystem I-reduced ferredoxin into a thiol signal that is transmitted to TRX through the action of FTR [12,13]. Under illumination, TRX becomes reduced and catalyzes the reduction of regulatory disulfide bonds controlling the activation state of CBC target enzymes [5,14].

TK is a potential candidate for redox regulation, being involved in multiple metabolic pathways as the connection between PPP and glycolysis, carbon fixation, and the biosynthesis of coenzymes, fatty acids, amino acids, glutathione and vitamins. However, there is no direct evidence that TK activity might be modulated by redox regulatory mechanisms [15], although proteomic surveys suggested that this enzyme could be a potential target of TRX [16-19].

3

In this work, we focused on the structural and biochemical characterization of chloroplastic TK from the green microalga *Chlamydomonas reinhardtii* (CrTK). In order to study the properties of this key enzyme, CrTK was heterologously expressed in *E. coli* and purified by metal affinity chromatography. Biochemical features of the enzyme were defined and its structure was determined by X-ray crystallography. Regulation by oxidative modifications and Mg^{2+} concentration were analyzed by activity assays and circular dichroism (CD). As observed for other TKs, we found a strong influence of Mg^{2+} on the reconstitution of the active holo enzyme. Our results suggest that fluctuations of the Mg^{2+} concentration have a strong impact on the CrTK activity and participate in the redox control of the enzyme by changing its propensity to be inactivated by oxidation.

2. Materials and Methods

2.1 Materials

All chemicals were obtained from Sigma-Aldrich unless otherwise specified. Desalting columns (NAP5 and PD-10) were purchased from GE Healthcare. Crystallization plates and silanized cover slips were purchased from Molecular Dimensions.

2.2 Plasmid construction for expression of CrTK and EcE4PDH in Escherichia coli

The cDNA-encoding chloroplastic transketolase from *C. reinhardtii* (CrTK) was amplified by PCR using a forward primer introducing an *Nde*I restriction site at the start codon (5′-AACGTGCATATGGCTCAGGCTGCCCCCGCT-3′); and a reverse primer introducing a *Bam*HI restriction site downstream of the stop codon (5′-ACCATGGGATCCTTAGTGCTGCAGGGTGGC-3'). CrTK is encoded by the gene at locus Cre02.g080200 and appears to be the only TK in *C. reinhardtii*. CrTK was cloned in a modified pET-3c vector containing additional codons upstream of the *Nde*I site to express a His-tagged protein with seven N-terminal histidines. This modified vector (pET-3c-His) was generated by restriction with *Xba*I and *Nde*I of pET-3c to insert the following sequence: 5'-TCTAGAAATAATTTTGTTTAACTTTAAGAAGGAGATATACAA<u>ATG</u>**CACCACCACCA CCACCACC***ATAT*G-3' (*Nde*I italicized, start codon underlined and seven His codons in bold). The recombinant CrTK contains 692 residues with an estimated molecular weight of 75,169.6 Da; it starts at the N-terminus with the introduced MHHHHHHHM peptide followed by the mature protein

sequence (*i.e.* upon removal of the chloroplast targeting sequence), beginning with Ala36 (Fig. S1). The plasmid encoding erythrose-4-phosphate dehydrogenase from *Escherichia coli* (EcE4PDH) was used as in [20].

2.3 Protein purification

Recombinant CrTK was produced in *E. coli* with the pET-3c–His/BL21 expression system. Bacteria were grown at 37 °C in LB medium supplemented with 50 µg mL^{-1} ampicillin; the expression of the protein was induced with 0.2 mM isopropyl-β-D-thiogalactopyranoside (IPTG) at 25 °C for 16-18 h when the culture reached an Abs$_{600}$ of 0.5. Cells were then harvested by centrifugation, re-suspended in 20 mM Tris-HCl (pH 7.9), 0.5 M NaCl, 5 mM imidazole (binding buffer), and disrupted by a double passage in a French Press Cell set at 1000 PSI. RNAse and DNAse (10 µg mL^{-1}) were then added to the suspension and let to digest nucleic acids for 20 min at room temperature. Residual cell debris were removed by centrifugation at 30,000 $\times$ *g* for 45 minutes. The supernatant was then applied onto a Ni^{2+} NTA column (Chelating Sepharose Fast Flow resin, GE Healthcare) pre-equilibrated with binding buffer. The column was washed with the same buffer containing increasing concentrations of imidazole (25, 60 and 100 mM) to remove contaminants. Finally, CrTK was eluted with binding buffer supplemented with 250 mM imidazole. Eluted fractions were desalted using PD10 columns (GE Healthcare) pre-equilibrated with 50 mM Tris-HCl (pH 7.9), 1 mM EDTA. Fractions were analyzed by SDS-PAGE and those containing pure CrTK concentrated by ultrafiltration in Centricon cartridge (Amicon, 10 kDa cut-off) and stored at –80 °C. The protein concentration was determined experimentally based on the UV absorption at 280 nm (A_{280}); the molar extinction coefficient of CrTK ($\varepsilon_{280} = 89,270$ M^{-1} cm^{-1}) was calculated assuming that cysteine residues are not involved in disulfide bonds [21]. EcE4PDH was purified following the same protocol described above, except that its expression was induced by addition of 0.2 mM IPTG at 30 °C for 16-18 h when the culture reached an Abs$_{600}$ of 0.5. The concentration of EcE4PDH was determined by UV spectroscopy ($\varepsilon_{280} = 32,430$ M^{-1} cm^{-1}).

2.4 Liquid chromatography-mass spectrometry analysis

The molecular weight of CrTK was evaluated by LC-ESI-MS analysis. The chromatographic analysis was performed on an Agilent 1200 HPLC system (Walbronn, Germany) using a monolithic CIMac C4 Analytical column (5 mm $\times$ 5.3 mm I.D.; BIA Separations, Ljubljana, Slovenia). Mobile phases A [water–acetonitrile-FA (99:1:0.1, v/v/v)] and B [water–acetonitrile-FA (2:98:0.1, v/v/v)] were used

to develop a gradient. The optimized mobile phase gradient was set as follows: A–B from (80:20, v/v) to (50:50, v/v) in 6 min; from (50:50, v/v) to (20:80, v/v) in 1 min; (20:80, v/v) for 1 min. The column was equilibrated with the mobile phase composition of the starting conditions for 3 min before the next injection. The flow rate was set at 0.5 mL/min. The injection volume was 2 µL corresponding to 0.7 µg of protein solubilized in 5 mM ammonium bicarbonate buffer at pH 7.9. MS analysis was carried out on a Q-ToF Micro quadrupole time-of-flight (Q-TOF) hybrid analyzer (Micromass, Manchester, UK) with a Z-spray electrospray ion source (ESI). The ESI-Q-TOF source temperature was set at 100 °C, the capillary voltage at 3.3 kV and the cone voltage at 35 V. The scan time was set at 2.0 s and the inter scan time at 0.1 s. The cone gas flow was set at 120 L h^{-1} and the desolvation gas at 500 L h^{-1}. Chromatograms were recorded in total ion current (TIC), within 800 m/z and 2000 m/z. The CrTK baseline-subtracted spectrum (m/z 1,300–2,000) was deconvoluted onto a true mass scale using the maximum entropy (MaxEnt1)-based software supplied with MassLynx 4.1 software. Output parameters were set as follows: mass range 20,000–100,000 Da; resolution 2 Da/channel. The uniform Gaussian model was used, with 0.5 Da width at half height.

2.5 Gel filtration

Gel filtration analysis was performed on a Superdex 200 HR10/300 GL column (GE Healthcare) connected to an ÅKTA Purifier system (GE Healthcare), previously calibrated with standard proteins, as described in [22]. The column was equilibrated with 50 mM Tris-HCl (pH 7.5), 150 mM KCl and 1 mM EDTA. The volume of loaded CrTK samples was 0.25 mL at a concentration of 1 mg mL^{-1} (12 µM). The protein was eluted at a flow rate of 0.5 mL min^{-1}. A control run was conducted using the tetrameric cytoplasmic glyceraldehyde-3-phosphate dehydrogenase from *Arabidopsis thaliana* (isoform 1, AtGAPC1) [23].

2.6 Reconstitution of the holoenzyme and activity assay

Before activity assays, CrTK samples in the apo-form (hereafter CrTK$_{apo}$) were desalted using NAP5 columns (GE Healthcare) pre-equilibrated with 50 mM Tris-HCl (pH 7.9). CrTK$_{apo}$ (2.9 mg mL^{-1}) was then incubated at 25 °C for variable times (5-300 min) in the presence of 0.7 mM TPP supplemented or not with different concentrations of $MgCl_2$ ranging from 0.05 to 8 mM (hereafter CrTK$_{TPP/Mg}$ and CrTK$_{TPP}$, respectively). The catalytic activity of CrTK forms was detected spectrophotometrically by a coupled enzymatic assay with EcE4PDH [24], in a mixture containing 50 mM Tris-HCl (pH 7.9), 0.1 mM TPP, 2.5 mM β-NAD, 15 mM $MgCl_2$, 5 mM $CaCl_2$, 2 mM DL-G3P,

12 mM F6P, 2.7 µM EcE4PDH. The reaction was started by the addition of pre-incubated CrTK samples (10-50 nM). Activity was monitored for 2 min and calculated from the increase in absorbance at 340 nm (NADH production) with a Jasco V-550 UV/Vis spectrophotometer. For each protein sample, we assessed the linear dependency of CrTK activity upon CrTK concentration and the rate of NADH production was only measured within linearity. The catalytic activity, expressed as mol_{NADH}/mol_{TK} s^{-1}, was calculated from the $\Delta Abs_{340}/min$ considering a molar extinction coefficient for NADH of 6.22 M^{-1} cm^{-1}.

2.7 Oxidant treatments

Before oxidative treatments, $CrTK_{TPP}$ and $CrTK_{TPP/Mg}$ were prepared as described above and diluted seven-times in 50 mM Tris-HCl (pH 7.9). After dilution, CrTK samples were incubated at 25 °C in the presence of 20 or 50 mM trans-4,5-dihydroxy-1,2-dithiane (DTTox). At the indicated times, an aliquot was withdrawn to assay the activity as described above. Control CrTK samples were directly diluted in buffer without the addition of DTTox.

2.8 Dynamic light scattering

Dynamic Light Scattering (DLS) measurements were performed employing a Malvern Nano ZS instrument equipped with a 633 nm laser diode. Samples consisted of $CrTK_{apo}$, $CrTK_{TPP}$ (0.7 mM TPP) and $CrTK_{TPP/Mg}$ (0.7 mM TPP plus 8 mM $MgCl_2$) and $CrTK_{apo}$ pre-incubated in the presence of 50 mM DTTox. All samples were at 12 µM CrTK in 50 mM Tris-HCl (pH 7.9). Protein samples were used in disposable polystyrene cuvettes (100 µL) of 1 cm optical path length. The reported hydrodynamic radii (R_h) have been averaged from the values obtained from five measurements, each composed of 10 runs of 10 seconds.

2.9 Circular dichroism spectroscopy

The CD analysis on CrTK samples was performed on a Jasco J-810 spectropolarimeter equipped with a PTC-423S Peltier-type temperature control system; measurements were carried out in a Hellma 115B-QS micro cell (1 cm pathlength, 400 µL volume) using a 2 sec data integration time, a 2 nm spectral bandwidth and an accumulation cycle of 3 spectra per measurement. $CrTK_{apo}$ sample (6.3 µM) was prepared in 5 mM Tris-HCl (pH 7.9) supplemented with 0.1 mM Na_2EDTA and 2 mM $MgCl_2$. $CrTK_{TPP/Mg}$ was prepared by direct addition of TPP to the $CrTK_{apo}$ sample inside the micro cell (final concentrations: [CrTK] = 5.6 µM, [TPP] = 55.6 µM). Samples were then analyzed at 25 °C

in the 400–250 nm spectral range using a 20 nm min^{-1} scanning speed.

The kinetics of TPP binding to CrTK was evaluated on a CrTK$_{TPP/Mg}$ sample (17.8 µM) prepared in 5 mM Tris-HCl (pH 7.9) supplemented with 220 µM TPP and 2.5 mM MgCl$_2$. The sample was analyzed at 25 °C in the 400–300 nm spectral range using a 50 nm min^{-1} scanning speed; measurements were performed at different times after TPP addition over a 20 h period. The effect of Mg^{2+} depletion on TPP binding to CrTK$_{TPP/Mg}$ was then evaluated by adding an excess of Na$_2$EDTA (8 mM); the measurement was carried out after 2 h incubation at 25 °C.

CD spectra were converted to molar units ($\Delta\varepsilon$) based on the total concentration of CrTK; the insurgence of induced CD (ICD) signals [25,26] upon TPP binding was evaluated by subtraction of the CD spectrum of CrTK$_{apo}$ from the CD spectra of CrTK$_{TPP/Mg}$ samples.

2.10 Crystallization and data collection

CrTK$_{apo}$ (without cofactors) and CrTK$_{TPP/Mg}$ (protein plus 0.25 mM TPP and 2 mM MgCl$_2$) were concentrated to 4.5 mg mL^{-1} in 50 mM Tris-HCl (pH 7.9), 1 mM EDTA and crystallized by the hanging drop vapor diffusion method at 293 K. The Structure screen 1 from Molecular Dimensions and the Crystallization Extension kit for Proteins from Sigma Aldrich, both based on the sparse matrix screen elaborated in [27] were used as starting screening. A protein solution aliquot of 2 µL was mixed to an equal volume of reservoir, and the prepared drop was equilibrated against 800 µL of reservoir. Small crystals and crystalline aggregates grew from various reservoirs of the Extension kit (*i.e.* 22: 12 % w/v PEG 20K, 0.1 M MES, pH 6.5; 30: 10 % w/v PEG 6K, 5 % v/v MPD, 0.1 HEPES, pH 7.5; 37: 10 % w/v PEG 8K, 0.1 M HEPES, pH 7.5; and 38: 20 % w/v PEG 10K, 0.1 M HEPES, pH 7.5). The crystallization conditions were optimized and the best crystals grew from a reservoir containing 10 % w/v PEG 6K, 5 % v/v MPD and 0.1 M MES pH 6.5-7.0 or 0.1 M HEPES pH 7.0-8.0. Crystals were mounted from the crystallization drop into cryo-loops, briefly soaked in a cryo-protectant solution containing 12 % w/v PEG 6K and 15 % v/v MPD, and then frozen in liquid nitrogen. Diffraction images were recorded at 100 K using a synchrotron radiation at Elettra (Trieste, beam line XRD1) for CrTK$_{TPP/Mg}$ and at the European Synchrotron Radiation Facility (Grenoble, beam line ID30B) for CrTK$_{apo}$. The data at a resolution of 1.74 Å for CrTK$_{TPP/Mg}$ and 1.58 Å for CrTK$_{apo}$ were processed using XDS [28] and scaled with SCALA [29]. The correct space group was determined with POINTLESS [29] and confirmed in the structure solution stage. The data collection statistics are reported in Table 1.

2.11 Structure solution and refinement

The CrTK$_{TPP/Mg}$ structure was solved by molecular replacement using the program MOLREP from CCP4 package [30]. The coordinates of TK from *Zea mays* (PDB code 1ITZ) [9], deprived of TPP, Mg^{2+} and water molecules, were used as search probe. Initial stages of the refinements were performed with CNS1.3 [31] selecting 5 % of reflections for R$_{free}$. The residual electron density map clearly showed the position of TPP and Mg^{2+}, which were added to the model. Water molecules were automatically added and, after a visual inspection, they were conserved in the model only if contoured at 1.0 σ on the ($2F_o - F_c$) map and if they fell into an appropriate hydrogen bonding environment. In the final stages of the refinement performed with REFMAC 5.5.0109 [32], alternate conformations, if visible, were inserted. The structure of CrTK$_{TPP/Mg}$ without TPP, Mg^{2+} and waters, was used as probe to solve the CrTK$_{apo}$ structure by molecular replacement using MOLREP [30]. The refinement was performed as described above for CrTK$_{TPP/Mg}$. The refinement statistics are reported in Table 1. The manual rebuilding was performed with Coot [33]; protein superimpositions were performed by LSQKAB from CCP4 package [30].

2.12 Accession numbers

The atomic coordinates and structure factors of CrTK$_{TPP/Mg}$ and CrTK$_{apo}$ structures have been deposited in the Protein Data Bank with the accession numbers 5ND5 and 5ND6.

3. Results

3.1 Magnesium and TPP are both fundamental to reconstitute fully active CrTK

The reconstitution of the fully active TKs isolated from different organisms shows a strong dependence on divalent cations and TPP [8,34,35]. Since the cofactor TPP and Mg^{2+} were lost during the purification procedure (see Material and Methods and below), we first analyzed the time-dependence of CrTK catalysis on CrTK reconstitution in the presence of over-saturating concentrations of TPP and Mg^{2+}. Samples of CrTK without cofactors (thereafter indicated CrTK$_{apo}$) were incubated at 25 ºC in reconstitution buffer containing 50 mM Tris-HCl (pH 7.9), 0.7 mM TPP and 8 mM MgCl$_2$. Activity was evaluated over-time (5-300 min) with a coupled enzymatic assay using fructose-6-phosphate (F6P) and glyceraldehyde-3-phosphate (G3P) as substrates. As shown in Fig. 1A, the enzyme activity increased over time, reaching its maximal value after ~3 h (~150-160

Fig. 1. **Reconstitution of the CrTK$_{TPP/Mg}$ active enzyme.** **(A)** Activities of CrTK samples reconstituted with 0.7 mM TPP and 8 mM MgCl$_2$. At the indicated times, an aliquot was withdrawn to measure CrTK activity following the procedure described in Materials and Methods. White square: activity of CrTK incubated in the absence of MgCl$_2$. The experimental data have been fitted with an arbitrary function and represent the mean ± SD of three replicates (n = 3). **(B)** Activities of CrTK samples reconstituted with 0.7 mM TPP and increasing Mg^{2+} concentrations. After 3 h incubation, the activity was measured following the procedure described in Materials and Methods. The experimental data have been fitted with an arbitrary function and represent the mean ± SD of three replicates (n = 3). The white square symbol refers to CrTK$_{TPP}$ reconstituted in the absence of Mg^{2+} (40 mol$_{NADH}$/mol$_{TK}$ s^{-1}). **(C)** Activities of CrTK reconstituted with 0.7 mM TPP (CrTK$_{TPP}$, white squares) or with 0.7 mM TPP supplemented with 8 mM MgCl$_2$ (CrTK$_{TPP/Mg}$, black squares). Activities of CrTK samples have been plotted as a function of Mg^{2+} concentrations in the assay buffer and normalized to the maximal activity (130 mol$_{NADH}$/mol$_{TK}$ s^{-1}) measured for the fully reconstituted enzyme (CrTK$_{TPP/Mg}$). The experimental data have been fitted with an arbitrary function and represent the mean ± SD of three replicates (n = 3).
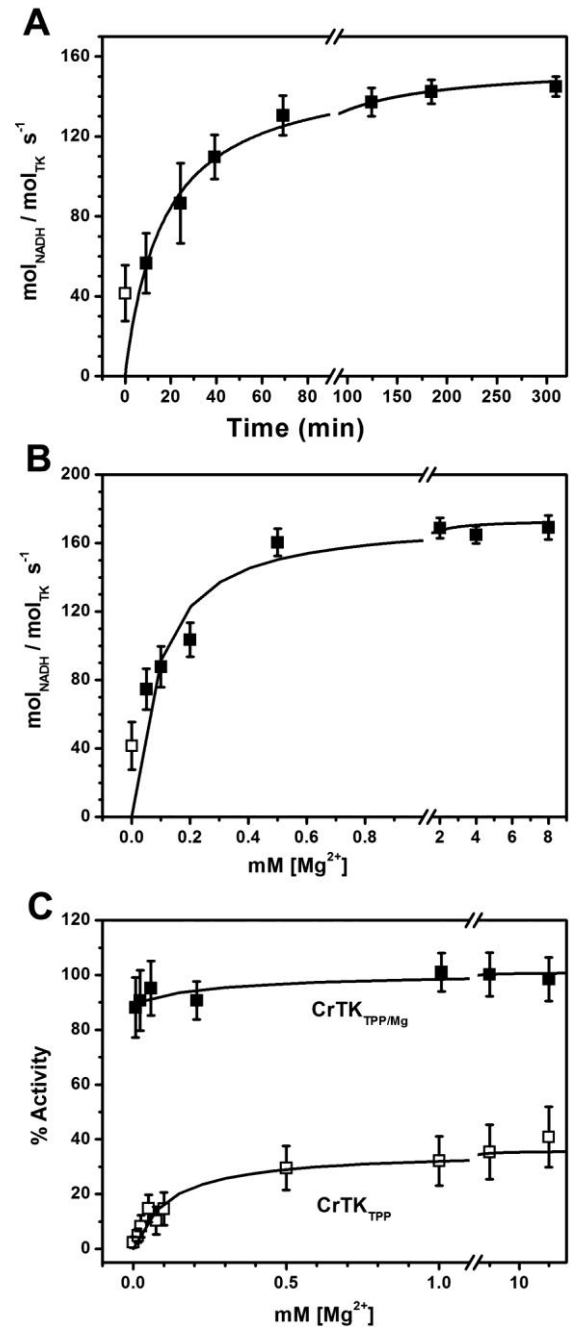
mol$_{NADH}$/mol$_{TK}$ s^{-1}). We then evaluated the dependence of the CrTK catalytic activity on CrTK reconstitution with over-saturating TPP and variable amount of Mg^{2+}. Samples of CrTK$_{apo}$ were incubated for 3 h at 25 °C in reconstitution buffer containing 50 mM Tris-HCl (pH 7.9), 0.7 mM TPP and different MgCl$_2$ concentrations ranging from 0 to 8 mM. After incubation, the activity was

measured as described above. As shown in Fig. 1B, incubation in the presence of Mg^{2+} significantly stimulated the activity of CrTK, and the enzyme attained its full activation (~150-160 mol_{NADH}/mol_{TK} s^{-1}) at Mg^{2+} concentration ≥ 1 mM. This value exceeds almost 20 times the stoichiometric amount required on the basis of monomer concentration. By contrast, the activity of $CrTK_{apo}$ incubated in the presence of TPP without Mg^{2+} (thereafter indicated $CrTK_{TPP}$) was 40 mol_{NADH}/mol_{TK} s^{-1} (Fig. 1B, white square), a value four times lower compared to fully reconstituted CrTK (thereafter indicated $CrTK_{TPP/Mg}$). In agreement with what reported about the activation of yeast TK [36], when $CrTK_{TPP}$ was not pre-incubated in the presence of Mg^{2+} the enzyme exhibited a lower activity, even if exposed to saturating concentrations of divalent cations (*i.e.* Mg^{2+} and Ca^{2+}) during the activity assays.

As the coupled assay used to measure CrTK activity was conducted at high concentrations of Mg^{2+} and Ca^{2+}, we have also determined the dependence of $CrTK_{TPP}$ and $CrTK_{TPP/Mg}$ activity as a function of Mg^{2+} concentration in the assay buffer deprived of calcium ions. As shown in Fig. 1C (black squares), $CrTK_{TPP/Mg}$ was not responsive to the presence of Mg^{2+}, showing 90% of maximal activity even in the absence of Mg^{2+} in the assay buffer. A different scenario is presented by $CrTK_{TPP}$ that displayed a strong sensitivity to Mg^{2+} in the assay buffer (Fig. 1C, white squares). Moreover, the activity of $CrTK_{TPP}$ measured under assay conditions deprived of Mg^{2+} was ~4 mol_{NADH}/mol_{TK} s^{-1} (Fig. 1C, first white square), a value representing 10% of the maximal activity reached at saturating Mg^{2+} concentration (Fig. 1C, white squares). As reported by Heinrich *et al* [8], we cannot exclude the presence of trace contaminant cations in the assay buffer due to the addition of substrates, or that the enzyme retains some activity even in the absence of Mg^{2+}. However, when we compared the activities of $CrTK_{TPP}$ and $CrTK_{TPP/Mg}$ in assay conditions deprived of Mg^{2+}, the former activity is extremely low, being only 3% of the activity measured for $CrTK_{TPP/Mg}$ (Fig. 1C, first white and black squares, respectively).

Altogether, these results indicate that maximal catalytic activity requires long-time incubation (at least 2 hours) of CrTK with over-saturating TPP and Mg^{2+} concentration. Indeed, CrTK reconstituted in the presence of TPP without Mg^{2+} (*i.e.* $CrTK_{TPP}$) does not reach the optimal catalysis activity even in the presence of over-saturating Mg^{2+} in the assay buffer.

3.2 Induced CD spectra of CrTK

Upon binding of TPP to TK from *S. cerevisiae*, an increase in absorption can be observed in the near UV range (285–360 nm) [1,37-39]. A peculiar bisignate induced CD (ICD) signal, closely related to the increase in UV absorption, is also observed across a variety of TPP-dependent enzymes [1,39,40].

CrTK$_{TPP/Mg}$ displays a bisignate ICD signal in the 380–260 nm range (Fig. 2A), with a negative band centered at 325 nm and a positive band centered at 275 nm; the ICD profile is very similar to those reported for other variants of TK. The binding of TPP to CrTK displayed a relatively slow kinetics: the intensity of the ICD signal increased with time, reaching saturation 3 h after addition of the cofactor (Fig. 2B) consistent with activity assays (Fig. 1A). Treatment of CrTK$_{TPP/Mg}$ with excess of the chelating agent Na$_2$EDTA caused the complete disappearance of the ICD signal of TPP (Fig. 2B): this behavior clearly demonstrated that Mg^{2+} is necessary for the effective formation of a CrTK/TPP complex in the most catalytically active configuration.
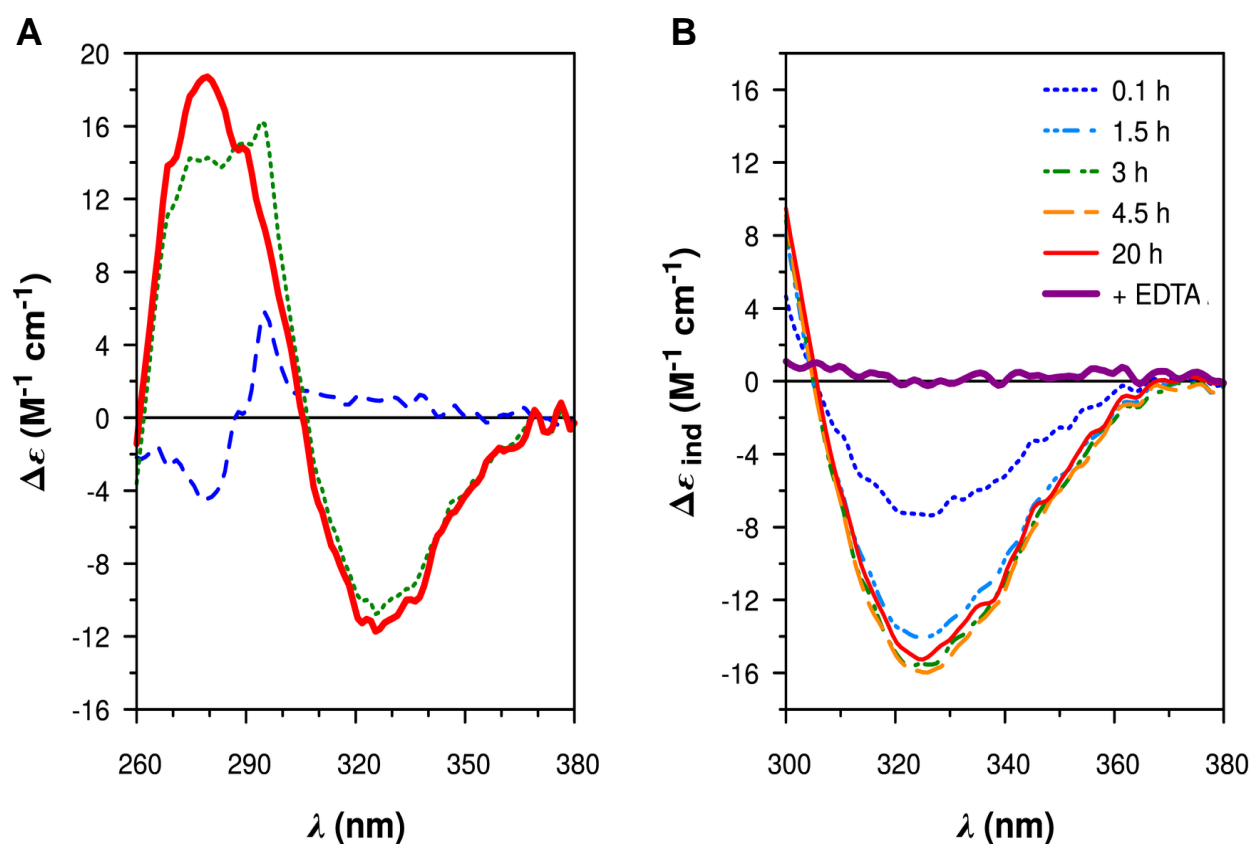
Fig. 2. ICD spectra for TPP binding to CrTK

(A) CD spectra for CrTK$_{apo}$ (6.3 µM; blue thin line) and CrTK$_{TPP/Mg}$ (5.6 µM, [TPP] = 55.6 µM; green dotted line); the resulting ICD signal for the binding of TPP to CrTK is shown (bold red line). **(B)** ICD spectra for the binding of TPP (220 µM) to a sample of 17.8 µM CrTK, 2.5 mM MgCl$_2$ at different times after TPP addition (thin lines) and after addition of 8 mM Na$_2$EDTA (bold purple line).

*3.3 Quaternary structure of CrTK$_{apo}$ and CrTK$_{TPP/Mg}$*

Based on the available structures of TKs, the enzyme is a homodimer composed by two identical subunits [6,9]. In order to investigate the oligomerization state of CrTK, we performed gel filtration experiments and DLS analysis. Even though that the purified CrTK$_{apo}$ is deprived of the cofactors Mg^{2+} and TPP (*i.e.* CrTK$_{apo}$), it eluted as a single symmetric peak with an apparent molecular mass of 156 kDa when analyzed by size-exclusion chromatography (Fig. S2). The elution behavior is similar to the well-known tetrameric enzyme AtGAPC1 (160 kDa) [23]. Since the molecular weight of the CrTK monomer determined by mass spectrometry is 75170 Da (Fig. S3), the CrTK appears as a homodimeric protein. The dimeric state of CrTK$_{apo}$ in solution was further confirmed by DLS measurements that reported a hydrodynamic radius of 5.1 ± 0.1 nm, corresponding to an apparent molecular mass of 151.6 ± 7.4 kDa (Table S1). DLS analysis was also employed to evaluate the effect of TPP and Mg^{2+} on the overall structure of CrTK. Under these conditions, CrTK remains homodimeric (Table S1).

3.4 Crystal structure of CrTK$_{apo}$ and CrTK$_{TPP/Mg}$

CrTK$_{apo}$ and CrTK$_{TPP/Mg}$ were crystallized as described in the Materials and Methods section. Both forms produced different polymorphs, belonging to C2 or P1 space groups (not shown). One crystal for each form was selected for the final structure determination on the basis of resolution and quality of the data (Table 1). Despite differing for unit cell dimensions, crystals of CrTK$_{apo}$ and CrTK$_{TPP/Mg}$ both belong to C2 space group and show a similar Matthews coefficient (2.32 and 2.42, respectively) and solvent content (47.1 % and 49.2 %, respectively). In both crystals, the asymmetric unit contains two protein chains related by a non-crystallographic two-fold axis and forming the V-shaped homodimer (Fig. 3A). In both forms, each monomer is formed by 670 amino acids, starting from Ser49 (the first residue visible in the electron density map), to the last C-terminal residue (His718) that could be modeled only in one subunit of CrTK$_{apo}$. To avoid misinterpretation with previous studies [5,41], amino acids of CrTK were numbered following the full-length enzyme (mature enzyme plus transit peptide; Fig. S1). As previously reported for other TK structures [6,9], each CrTK monomer is composed of three consecutive α/β domains all containing a central five stranded β-sheet (Fig. 3B). The N-terminal domain (residues 49-372) folds in a parallel β-sheet composed of strands β1, β2, β3, β6 and β7 surrounded by several α-helices (α1-α12; Fig. S4). It binds the Mg^{2+} ion and the pyrophosphate moiety of TPP, therefore it is called PP domain (Fig. 3B). The middle domain

(residues 373-582) is also composed of a parallel β-sheet (β9-β13) embedded in several helices from α13 to α18 (Fig. S4). This domain binds the cofactor pyrimidine ring of the adjacent monomer and is called Pyr domain (Fig. 3B). The C-terminal domain (residues 583-718) is the smallest domain and it folds in a mixed β-sheet with four parallel strands (β16-β19), one antiparallel strand (β15), and several α-helices (α19 to α25). This domain is not involved either in dimer interface or in the cofactor binding (Fig. 3B). The CrTK structure is characterized by long α-helix regions but it contains also several short 3_{10} and π helices connecting different secondary structure elements.

Fig. 3. Ribbon representation of CrTK$_{TPP/Mg}$ structure (A) View of the V-shaped dimer including the two cofactors TPP and Mg^{2+} present in each monomer. The two monomers are differently colored. The TPP (red) is shown as sticks and the Mg^{2+} (green) as sphere. **(B)** View of the dimer including TPP shown as sticks and the Mg^{2+} as green sphere. The three domains of one monomer are differently colored: N-terminal or PP domain in cyan, the middle or Pyr domain in green and the C-terminal domain in red. One TPP interacts with the PP domain (cyan) by the pyrophosphate groups; the second TPP interacts with the Pyr domain (green) by the pyrimidine ring. Atom colors: yellow (C), blue (N), red (O), purple (P) and green (Mg). The figure was prepared with Pymol (The PyMOL Molecular Graphics System, Version 1.5.0.5 Schrödinger, LLC).
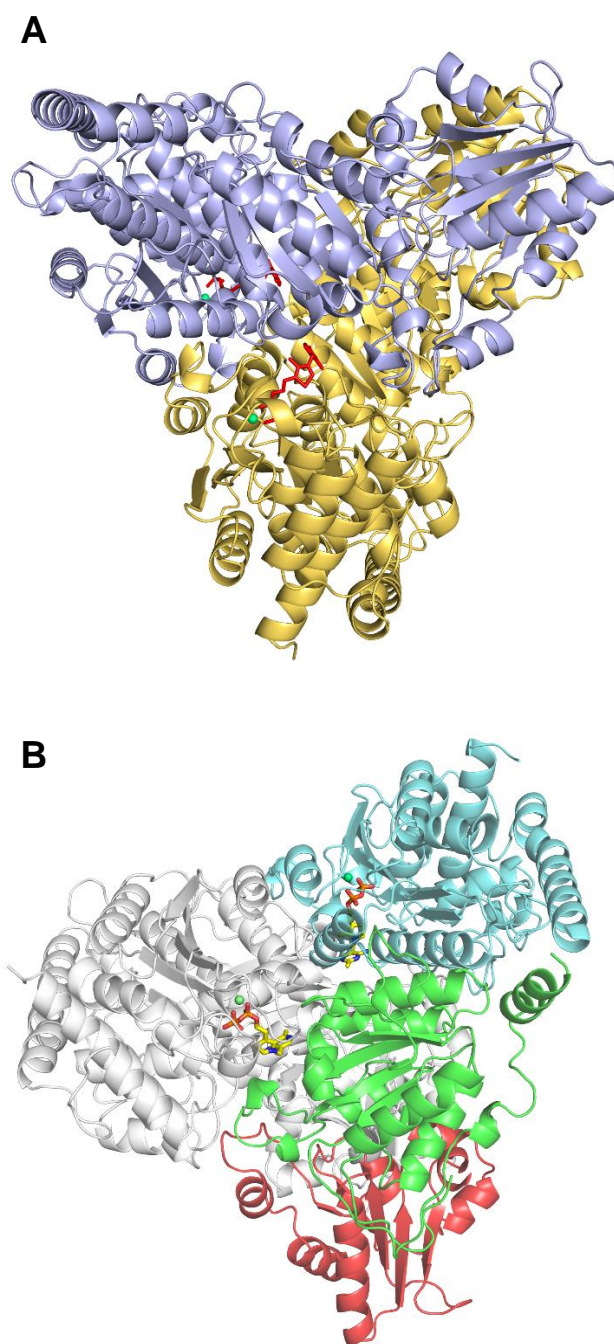
3.5 Comparison of CrTK with other TK structures

The three-dimensional structure of TK from *Zea mays* (PDB code 1ITZ) [9] is the unique TK structure from a photosynthetic organism present in PDB. CrTK shares with this protein a sequence identity of about 65%. Superimposition of C_α atoms based on secondary structure matching, results in a root mean square deviations (rmsd) of 0.9 Å on 1320 aligned residues (whole dimer) and 0.8 Å on 663 aligned residues (single monomer) indicating that the TK structure is highly conserved between the two organisms. While the internal β-sheets of N-terminal and middle domains are well superimposed, some deviations can be observed in correspondence to the solvent exposed helices α12 and α13 and the C-terminal domain (Fig. S5A). Moreover, the N-terminal and the middle domains of the two structures superimpose with rms deviations of 0.6 Å (on 322 aligned residues) and 0.7 Å (on 209 aligned residues), respectively, while the C-terminal domain does with a slightly higher rmsd (0.9 Å on 132 aligned residues).

In the case of the yeast enzyme (PDB code 1TRK) [6], the sequence identity with CrTK is about 53%. The rmsd from the superimposition of Cα atoms based on secondary structure matching increases to 1.2 Å on 1295 aligned residues (whole dimer) and 1.1 Å on 651 aligned residues (single monomer) with respect to the previous comparison. Differences are mainly observed in the correspondence to some exposed regions of the N-terminal domain, in particular in the region comprising helices α10, α11, α12 and α13 (Fig. S5B). In this case, the superimposition of N- and C-terminal domains gives higher deviations (1.1 Å on 313 aligned residues and 1.2 Å on 127 aligned residues, respectively) with respect to that one of middle domains (0.9 Å on 210 aligned residues).

3.6 CrTK$_{TPP/Mg}$ structure reveals multiple interactions between TPP, Mg^{2+} and active site residues

In the CrTK$_{TPP/Mg}$, each subunit binds one TPP molecule and one Mg^{2+} ion in the active site cleft at the dimer interface. The TPP and the Mg^{2+} are set in place by hydrogen bonds involving residues of both subunits and water molecules (Fig. 4 and Table S2).

Fig. 4. Two-dimensional diagram of interactions between TPP and CrTK residues. Protein residues, TPP, Mg^{2+} and waters are shown in ball-and-stick representation. Hydrogen bonds are shown as green dotted lines and their length is indicated in Å, while the spoked arcs represent protein residues making non-bonded contacts with the ligand. Atom colors: black (C), blue (N), red (O), yellow (S), purple (P) and green (Mg). The water oxygens are represented as pink spheres. The image was prepared using the software Ligplot+ v1.4.5 [74].

In particular, the phosphate groups of the TPP pyrophosphate moiety are stabilized by the N-terminal domain of one subunit, while the pyrimidine and the thiazolium rings interact with the middle domain residues of the adjacent subunit (Fig. 3B). Both rings are stabilized in the active site mainly by hydrophobic interactions: the thiazolium ring interacts with the side chains of Leu168 and Ile242 of

the same subunit and Leu433 of the adjacent subunit, while the pyrimidine ring is stacked between Leu168 of the same subunit and Phe490 of the adjacent subunit (Fig. 5A). Moreover, the hydrophobic cavity is also completed by Pro167, Val461, Leu433, Phe487 and Tyr493 from the two subunits (Fig. 5A). The N1 nitrogen atom of the pyrimidine ring is hydrogen bonded to the carboxyl oxygen OE2 of the strictly conserved residue Glu463 (Fig. 4 and Table S2) [42,43]. In addition, the N4 atom of the pyrimidine ring forms an intramolecular interaction with the C2 carbon of the thiazolium ring (Fig. 5A and Table S2) which favors the V-like conformation of TPP after binding and the C2 deprotonation required for catalysis [9,44].

Mg^{2+} shows an octahedral coordination with six oxygen atoms as electron donor, belonging to the pyrophosphate groups of TPP (O1B and O2A), the carboxylic group of Asp208 (OD2), the amide group of Asn238 (OD1), the main chain carbonyl group of Ile240 and a water molecule (Fig. 5B).
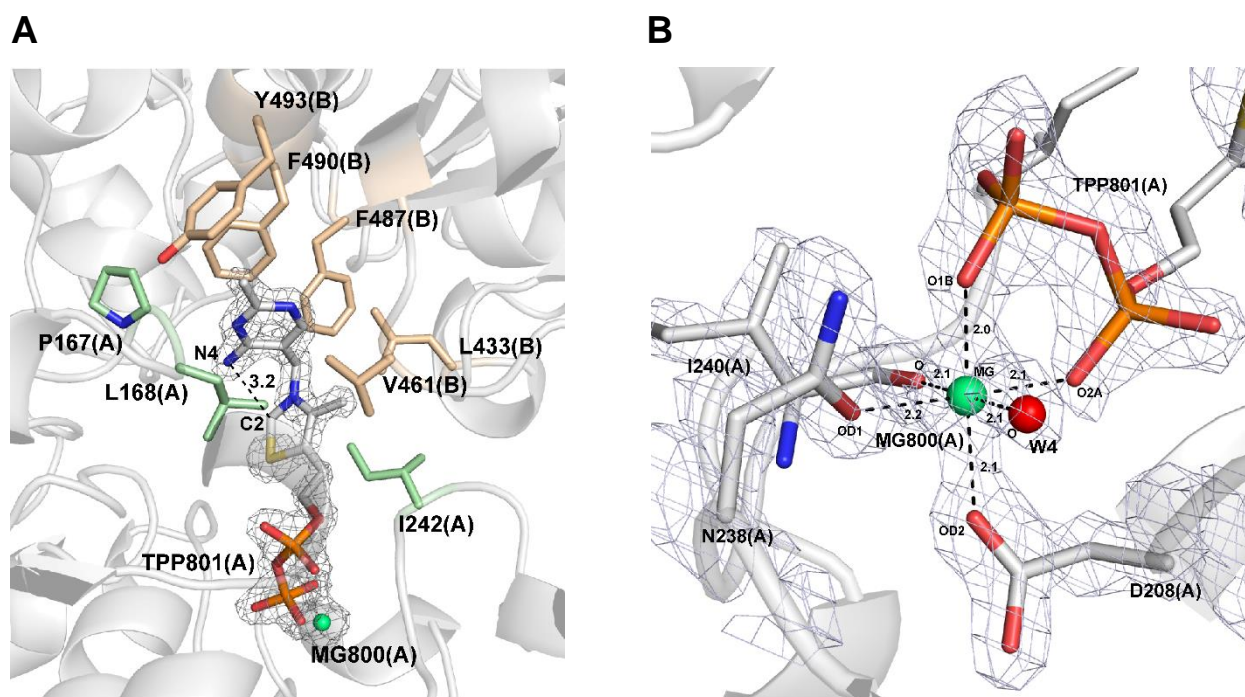

Fig. 5. Hydrophobic interactions of TPP and coordination site of Mg ion. (A) $2Fo - Fc$ electron density map contoured at 2σ around TPP. The pyrimidine and the thiazolium rings are stabilized by several protein residues of both subunits (A in light green, B in pale brown) forming a hydrophobic cavity. The side chain of Phe490 is in stacking interaction with the TPP pyrimidine ring. (B) $2Fo - Fc$ electron density map contoured at 1.5σ around Mg^{2+} and its ligands. The Mg^{2+} shows an octahedral coordination with six oxygen atoms as electron donors. Mg^{2+} is represented as a green sphere, the ligands as ball-and-stick. Atom colors: grey (C), blue (N), red (O) and orange (P). The figure was prepared with Pymol (The PyMOL Molecular Graphics System, Version 1.5.0.5 Schrödinger, LLC).

3.7 Comparison between CrTK$_{apo}$ and CrTK$_{TPP/Mg}$

In the CrTK$_{apo}$, the cleft displays no electron density attributable to TPP and Mg^{2+} supporting the fact that the purified protein before reconstitution is cofactor(s) free. By superimposing C$_\alpha$ atoms of CrTK$_{apo}$ and CrTK$_{TPP/Mg}$ monomers (chains A and B) and dimers, rmsd of 0.3 Å and 0.4 Å (on 667 and 668 superimposed atoms) and 0.4 Å (on 1335 superimposed atoms) are observed, respectively. Despite the high similarity between the two forms, in the CrTK$_{apo}$ two regions ranging between residues 239-247 and 433-437 (Fig. S4) are completely deprived of electron density, indicating that these regions are likely disordered and flexible (Fig. 6A). In CrTK$_{TPP/Mg}$ structure both regions are involved in TPP and Mg^{2+} binding (Fig. 6B) as for example the main chain carbonyl group of Ile240 which is hydrogen bonded to both TPP pyrophosphate O1B atom and Mg^{2+} (Fig. 4, Fig. 5B and Table S2) or the side chains of Ile242 and Leu433 stabilizing the TPP aromatic rings by hydrophobic interactions. CrTK$_{apo}$ structure shows that TPP is replaced by several water molecules located in the region of phosphate groups (W214, 450, 526, 557 and 751 in chain A and W366, 493 and 643 in chain B) and pyrimidine ring (W284, 496 and 559 in chain A and W172, 300 and 530 in chain B), whereas the Mg^{2+} site is empty (Fig. 6C). These molecules contribute mainly by hydrogen bonds to the stabilization of active site residues lying almost in the same position in the CrTK$_{TPP/Mg}$ structure, except for the two protein portions mentioned above. Both protein regions, disordered in CrTK$_{apo}$ structure, are also involved in dimer interface in CrTK$_{TPP/Mg}$ structure. Indeed, Ser241, Ile242 and Asp243 of one subunit interact with the carboxylate group of Asp432, the main chain nitrogen of Ala434 and the amino group of Arg458 of the other subunit (Fig. 6D). The absence of TPP probably induces a disorder in the region from residues 239 to 247 causing the impairment or the loss of the hydrogen bonds with residues 433-437 of the other subunit. In consequence, this second region more exposed to the solvent becomes flexible and disordered. To further investigate whether the presence/absence of TPP/Mg^{2+} (*i.e.* absence/presence of disordered regions) influences the protein stability, we evaluated the thermal-induced denaturation of CrTK$_{apo}$ and CrTK$_{TPP/Mg}$. Protein activities have been measured after 30 min exposure to increasing temperature ranging from 20 °C to 60 °C. CrTK$_{apo}$ has a T$_{50}$ (temperature causing 50% inactivation) of around 37 °C while this value is shifted to ~45 °C for CrTK$_{TPP/Mg}$ (Fig. S6). Moreover, at 40 °C the activity of the CrTK$_{TPP/Mg}$ sample was still maximal while the CrTK$_{apo}$ was almost completely inactivated. This indicates that the presence of TPP/Mg^{2+} in the active site stabilizes the enzyme when exposed to denaturing temperatures, suggesting that a significant decrease of the overall disorder/flexibility is due to TPP and Mg^{2+} binding.
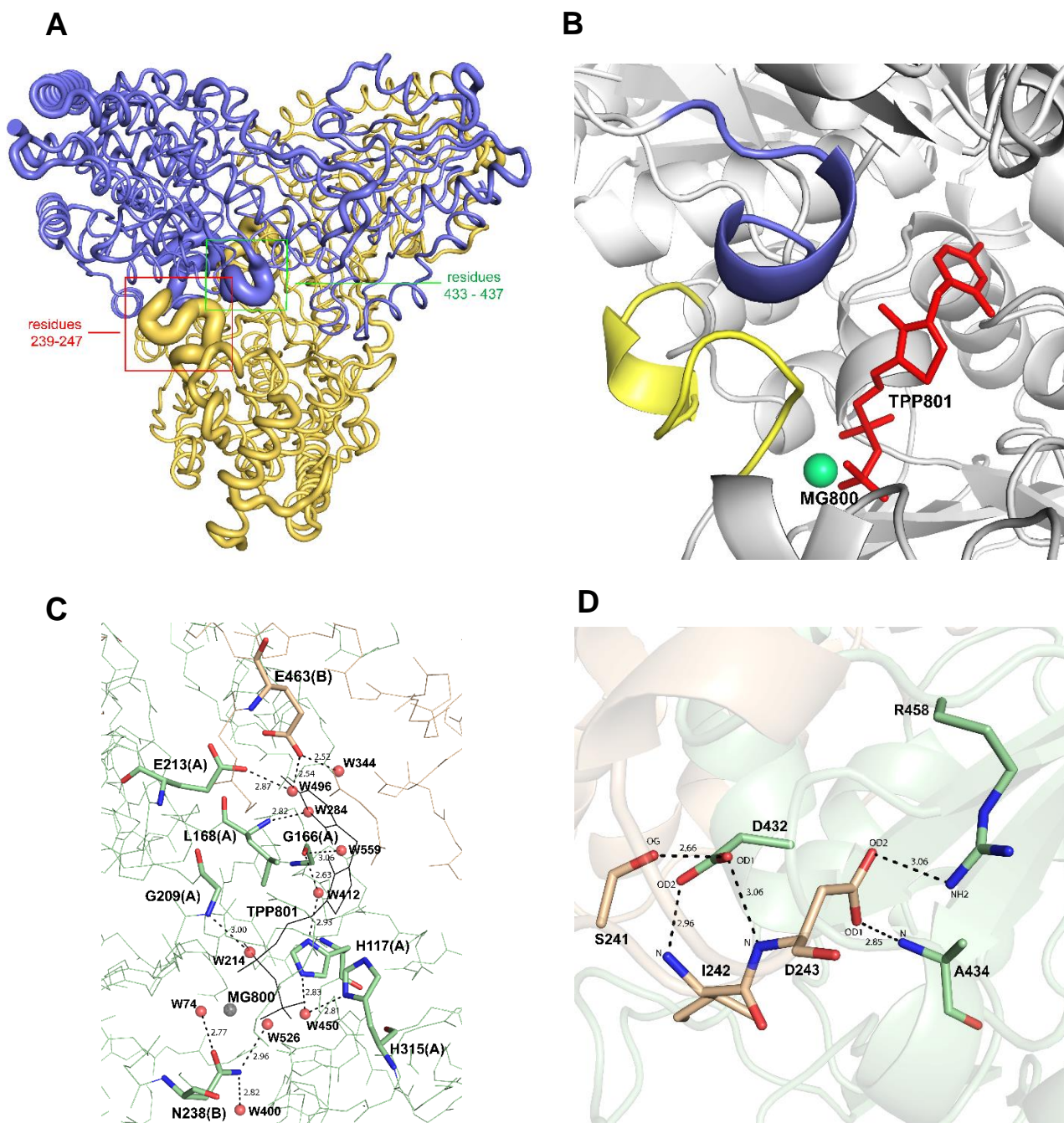
18

Fig. 6. Comparison between CrTK_apo and CrTK_TPP/Mg structures. (A) Representation of the CrTK_apo dimer structure. The thickness is correlated to the atom thermal factor (B-factor). The highlighted protein regions (239-247 and 433-437) are disordered and flexible. **(B)** CrTK_TPP/Mg structure reveals that the same protein regions have an ordered conformation and interact with TPP and Mg^{2+}. **(C)** CrTK_apo active site structure shows that water molecules occupy the position of TPP in CrTK_TPP/Mg structure (represented by grey thin lines for TPP and sphere for Mg^{2+}) and stabilize catalytic residues by hydrogen bonds. **(D)** Dimer interface in CrTK_TPP/Mg structure showing the interactions between the residues belonging to regions 239-247 and 433-437, disordered in CrTK_apo structure. The figure was prepared with Pymol (The PyMOL Molecular Graphics System, Version 1.5.0.5 Schrödinger, LLC).

19

3.8 Effect of DTT oxidation on CrTK activity

Plant TK was previously identified as putative target of TRX-dependent regulation [5] but no biochemical studies confirmed the sensitivity of this enzyme to dithiol/disulfide exchange reactions. Mature CrTK (CrTK sequence deprived of chloroplast transit peptide) enumerates twelve cysteines (Fig. 7A) mainly distributed in the PP and Pyr domains (Cys58, 84, 173, 204, 210, 220 and 366 in the PP domain; Cys386, 470, 484 and 582 in the Pyr domain) with only Cys638 located in the C-terminal domain (amino acids numbering refers to the full-length CrTK, Fig. S1). Among them, only cysteine residues at position 84, 210, 220, 470 and 484 are conserved in photosynthetic organisms (Fig. S4). Crystal structures of both CrTK$_{apo}$ and CrTK$_{TPP/Mg}$ show that all cysteines are in a reduced state making CrTK a putative target of oxidative regulation.

The analysis of CrTK$_{TPP/Mg}$ structure shows that the thiol sulfur atoms of Cys470 and Cys484 are located only 4.0 Å apart, while the distances Cys173 - Cys220 and Cys204 - Cys210 are 6.6 Å and 7.0 Å, respectively (all distances refer to the sulfur atoms; Fig. 7B). The thiol sulfur atoms of all other cysteine pairs lye at distances higher than 10 Å. These distance values do not significantly vary in CrTK$_{apo}$ structure (Cys470 SG - Cys484 SG = 4.1 Å, Cys173 SG - Cys220 SG = 6.7 Å and Cys204 SG - Cys210 SG = 7.0 Å). Thus, these residues may participate to the formation of regulatory disulfide bonds.
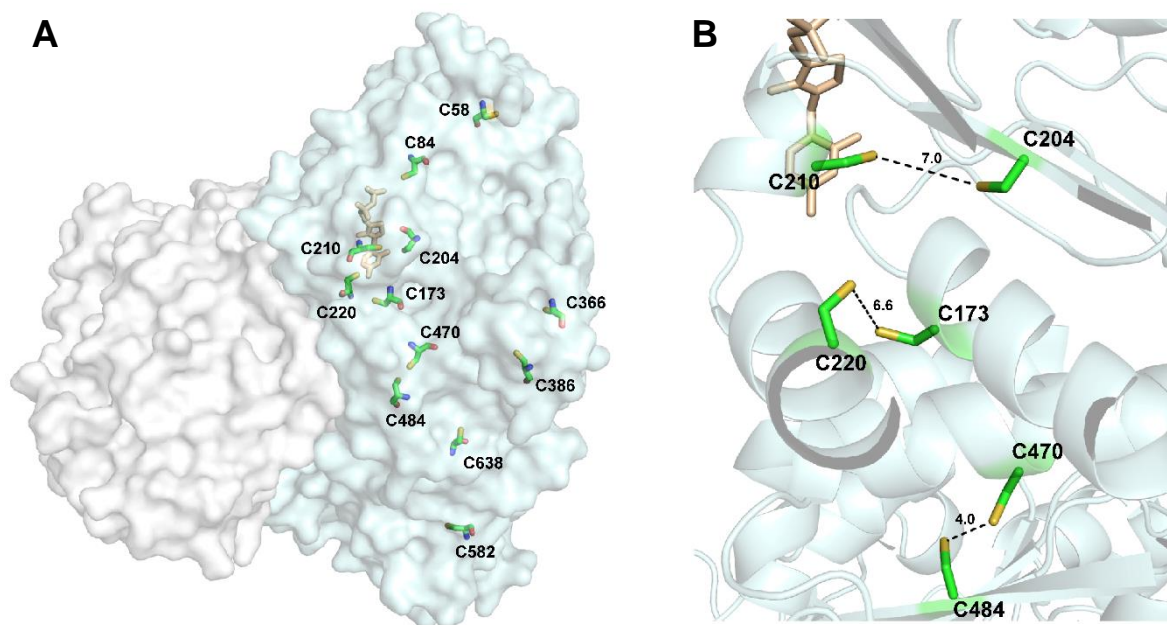

**Fig. 7. Cysteine residues in CrTK$_{TPP/Mg}$ structure**

(A) Position of cysteine residues in CrTK structure. Cys58, 84, 173, 204, 210, 220 and 366 are located in PP domain;

Cys386, 470, 484 and 582 in Pyr domain and Cys638 in C-terminal domain. Cysteines and TPP are represented in ball-and-stick, the two protein subunits as surface (chain A in light-cyan and chain B in gray). (B) Three pairs of cysteines belonging to chain A, show the thiol sulfur atoms ~~groups~~ at a distance < 10 Å. Atom colors: green (C), blue (N), red (O) and yellow (S). The figure was prepared with Pymol (The PyMOL Molecular Graphics System, Version 1.5.0.5 Schrödinger, LLC).

To test the sensitivity of CrTK activity to oxidative conditions, we exposed $CrTK_{apo}$, $CrTK_{TPP}$ and $CrTK_{TPP/Mg}$ to oxidized DTT (DTTox), an oxidant molecule known to induce disulfide formation. After 3 h incubation, the activity of $CrTK_{TPP/Mg}$ was almost unaffected, retaining more than 90% of the control (reduced) enzyme activity (Fig. 8A, left bars).

Fig. 8. **Oxidation of CrTK samples.**

(A) $CrTK_{apo}$, $CrTK_{TPP}$ and $CrTK_{TPP/Mg}$ samples were prepared following the procedure described in Material and Methods. After incubation, each sample was divided in two aliquots and diluted seven-times in 50 mM Tris-HCl (pH 7.9), in the presence (gray bars) or absence (white bars) of 50 mM DTTox. After 3 h incubation, the activity was measured following the procedure described in Materials and Methods. Data represent the mean percentage ± SD ($n = 3$). **(B)** $CrTK_{apo}$ was reconstituted in 50 mM Tris-HCl (pH 7.9) in the presence of 0.7 mM TPP, and variable Mg^{2+} concentrations. After 3 h incubation, each sample was treated as described in (A) and after additional incubation (3 h), the activity was assayed following the procedure described in Materials and Methods. The ratios between the activity of the oxidized and reduced (control) sample are plotted as a function of the Mg^{2+} concentration. The experimental data have been fitted with an arbitrary function and represent the mean ± SD of three replicates (n = 3).
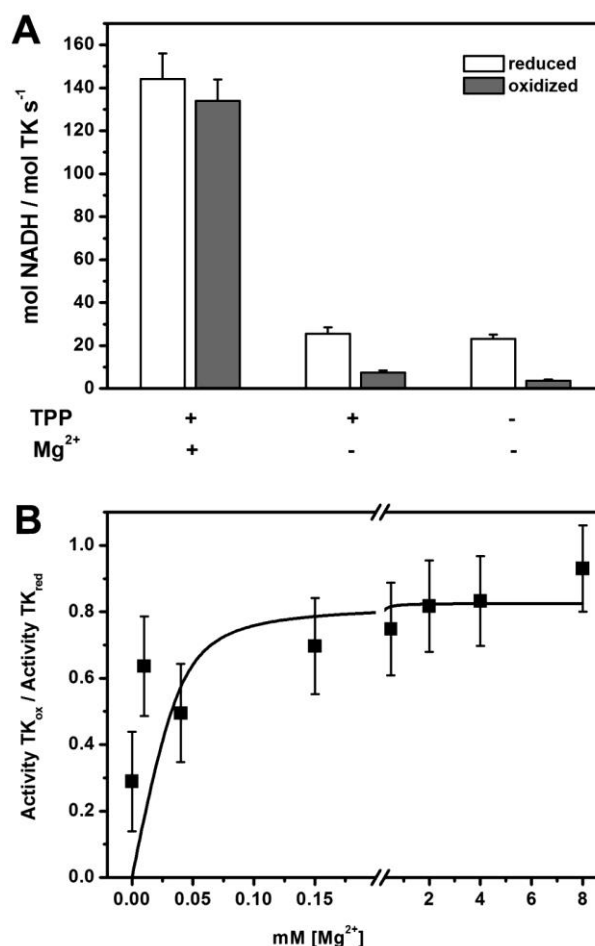
Thus, the oxidation induced by DTTox does not substantially influence the catalytic activity of the

21

fully reconstituted enzyme. Although its activity is 4-fold lower compared to the fully reconstituted enzyme (CrTK$_{TPP/Mg}$, Fig. 1B), CrTK$_{TPP}$ is strongly inhibited by oxidation, retaining only 20-30 % of its control activity when exposed to 50 mM DTTox (Fig. 8A, central bars and Fig. S7). A similar result was observed for the CrTK$_{apo}$, being 80% inactivated following incubation in the presence of identical amount of DTTox (Fig. 8A, right bars). Incubation of oxidized CrTK$_{TPP}$ with the strong reducing agent tri-carboxy-ethyl-phosphine (TCEP) [45] completely restored the activity, indicating that enzyme inhibition is due to reversible modifications such as disulfide bond(s) (Fig. S7). To better investigate the influence of the Mg^{2+} on the DTTox-induced inactivation of the enzyme, CrTK$_{apo}$ was reconstituted in the presence of TPP and variable concentrations of Mg^{2+}. Protein samples were then incubated in the absence or presence of DTTox. By plotting the ratios between oxidized and control activities against Mg^{2+} concentration, we noticed that the decrease of the Mg^{2+} amount in the reconstitution buffer is at the same time followed by an increased sensitivity of the enzyme to the oxidizing conditions (Fig. 8B). Taken together, these results indicate that only the CrTK$_{apo}$ and CrTK$_{TPP}$ forms are prone to oxidation-induced inhibition, and suggest that fluctuations of the Mg^{2+} concentration can modulate the extent of the enzyme sensitivity to oxidative regulation by influencing the relative amount of CrTK$_{TPP/Mg}$.

4. Discussion

The activity of TK isolated from diverse organisms is strictly dependent upon the presence of divalent cations and TPP [8,34,35,46]. The aim of the present study was to investigate the role of Mg^{2+} in the catalysis and regulatory mechanisms of CrTK and to get insight into the structural features of the enzyme. We focused our attention on the importance of Mg^{2+} ions because, in photosynthetic organisms, one of the documented effects induced by the transition from dark to light conditions is an increase of the magnesium concentration in the chloroplast stroma [47,48].

The reconstitution of fully active CrTK in the presence of an excess of TPP and Mg^{2+} requires long-time incubations (Fig. 1A) and is dependent on Mg^{2+} concentration in the pre-incubation media (Fig. 1B). Moreover, the activity of CrTK$_{TPP/Mg}$ is not affected by the absence of Mg^{2+} in the reaction assay (Fig. 1C). By contrast, the activity of CrTK$_{TPP}$ is sensitive to increasing concentrations of Mg^{2+} in the assay buffer but its maximal activity was 4-fold lower compared to the activity of CrTK$_{TPP/Mg}$ (Fig. 1B). This suggests that the transition from the partially active CrTK$_{TPP}$ to the fully active CrTK$_{TPP/Mg}$ is a slow process that does occur during long incubation of the enzyme with

over-saturating concentration of both TPP and Mg^{2+}. Indeed, short exposure of the $CrTK_{TPP}$ to Mg^{2+} ions during activity assay (2 min) is not sufficient to allow the enzyme to adopt suited conformation for optimal catalysis. This agrees with previous studies that analyzed the rate of transition from the apo-form of yeast TK to the fully active holo-form, demonstrating that the long time needed to reach the maximal activity is strongly decreased upon pre-incubation of the protein with both TPP and Mg^{2+} [8,36]. The formation of fully reconstituted TPP-dependent enzymes can be monitored by the appearance of UV and ICD signals upon TPP binding [39]. ICD spectra stem from the perturbations to the symmetry and electronic structure of a non-chiral ligand (*i.e.* TPP) interacting with a chiral guest [25,26]. In the case of TPP, these perturbations are due to the stabilization of the 4'-imino-1',4'-dihydropyrimidine tautomer of TPP, which is considerably less stable in aqueous solution than the 4'-aminopyrimidine tautomer, but is stabilized by the hydrophobic environment inside the catalytic site [38,49] and by the interaction with the highly conserved Glu463 (Fig. 4 and Fig. S4; Glu418 in yeast TK, [40]). Upon binding, TPP assumes a V-like conformation dictated by the optimal mutual orientation of the thiazole and pyrimidine rings for the effective deprotonation at C2 on the thiazole ring [50-52]. Consequently, these spectroscopic features arise from the catalytically active configuration of TPP and their intensities are linearly correlated to the catalytic activity of the enzyme [53,54]. A bisignate ICD signal in the 380–260 nm range was observed upon TPP addition to CrTK incubated in the presence of over-saturating amounts of $MgCl_2$ (Fig. 2A). In agreement with activity data (Fig. 1A), this ICD signal evolves with time, reaching its maximum in about 3 hours (Fig. 2B), showing that the transition from $CrTK_{apo}$ to $CrTK_{TPP/Mg}$ is a slow process. The chelating agent EDTA fully abolished the ICD signal (Fig. 2B), indicating that Mg^{2+} is fundamental for the correct binding of TPP inside the active site. Indeed, the $CrTK_{TPP/Mg}$ crystal structure shows that the metal ion is coordinated by 2 oxygen atoms of the TPP pyrophosphate moiety (Fig. 4 and Fig. 5A) as already reported for yeast and maize TKs [9,55]. Taken together, the biochemical and structural results indicate that Mg^{2+} is strictly required for optimal enzyme functioning and stabilizes the binding interaction between TPP and the enzyme, allowing the active site to assume the optimal configuration for the catalytic activity. By contrast, TPP alone is not sufficient to allow CrTK to reach its fully active state (Fig. 1B).

The comparison between the two limit structures in terms of activity (*i.e.* $CrTK_{apo}$ and the fully active $CrTK_{TPP/Mg}$) showed that the general fold is highly conserved except for two different portions (residues 239-247 and 433-437) which are completely disordered and flexible in $CrTK_{apo}$ (Fig. 6A) as previously reported for yeast TK [56]. The $CrTK_{TPP/Mg}$ structure highlighted that these protein

regions are involved in cofactors binding and they fold in an ordered conformation composed by short helices and random coil segments only in the presence of TPP and Mg^{2+} (Fig. 6B). Moreover, these two regions are located at the dimer interface and they form inter-chain interactions in $CrTK_{TPP/Mg}$ (Fig. 6D) that are absent in $CrTK_{apo}$. The results of the thermal stability comparison between $CrTK_{apo}$ and $CrTK_{TPP/Mg}$ agree with the structural observations. Notably, $CrTK_{TPP/Mg}$ showed a T_{50} significantly higher than $CrTK_{apo}$, indicating that the presence of TPP and Mg^{2+} in the active site decreases CrTK flexibility and stabilizes the protein towards thermal denaturation (Fig. S6). Therefore, we can propose that Mg^{2+}-dependent reconstitution/activation of CrTK is a slow process accompanied by protein conformational changes that allow a correct orientation of the cofactor TPP inside the catalytic center of the enzyme. Consistently, the formation of $CrTK_{TPP/Mg}$ can support maximal catalysis (Fig. 1). It has been already reported for yeast TK that the transition from the apo-protein to the fully active enzyme is a multi-step process, having a rate determined by slow rearrangements of the protein due to cofactor binding [1].

The dithiol/disulfide interchanges represent the main mechanism involved in the control of the activity of Calvin-Benson cycle (CBC) enzymes during light-dark transitions [5]. The formation of regulatory disulfides is accompanied by structural changes that modulate the activity of CBC enzymes allowing partial or complete inactivation. The regulation of CBC enzymes also involves other factors including light-dependent fluctuations of Mg^{2+} concentration [47,48,57,58]. In the last decades, several proteomic studies identified plant TK as a putative target of TRX-mediated regulation [16,17,19,59], suggesting the possible existence of regulatory cysteine residue(s). However, no biochemical study confirmed the TK sensitivity to redox transitions. The structures of CrTK here presented, reveal three putative cysteine couples (Cys173-Cys220, Cys204-Cys210 and Cys470-484) whose thiol sulfur atoms lye at distance lower than 10 Å, potentially involved in the formation of regulatory disulfide bonds (Fig. 7B). Moreover, we demonstrated that CrTK is sensitive to oxidative deactivation *in vitro* but this regulatory process is dependent on Mg^{2+}. Indeed, this metal preserves the fully active $CrTK_{TPP/Mg}$ from the inactivation induced by DTTox treatment (Fig. 8), likely precluding the formation of one or more regulatory disulfide bond(s). By contrast, both $CrTK_{apo}$ and $CrTK_{TPP}$, which lack Mg^{2+} in their active sites, are strongly sensitive to reversible inhibition by oxidation (Fig. 8 and Fig. S7). The role of Mg^{2+} in modulating such oxidative regulation is also suited to the physiological context. In fact, it has been previously reported that stromal Mg^{2+} concentration is in the low millimolar range [60], and varies according to several factors including light conditions [61,62]. It is well known the stromal pH increases upon illumination, and the transfer

24

of protons across the thylakoid membrane is believed to be electrically compensated by Mg^{2+} whose concentration increases in the stroma since the chloroplast envelope is relatively impermeable to this metal ion [63-65]. The stromal Mg^{2+} concentration is considered to increase 3- to 4-fold upon illumination [48,66]. This light-dependent fluctuation perfectly correlates with the strong dependency of CrTK activation upon increasing Mg^{2+} and oxidative inactivation observed under decreasing Mg^{2+} concentrations. The Mg^{2+}-dependent activation of CrTK and the role of Mg^{2+} in the modulation of oxidative sensitivity are reminiscent of the regulation of two other CBC enzymes, namely fructose-1,6-bisphosphatase (FBPase) and sedoheptulose-1,7-bisphosphatase (SBPase). Indeed, both enzymes are well known to be activated by Mg^{2+}, and this feature participates in the light-dependent activation of the enzymes [57,72]. This regulation was also found to act in concert with TRX-dependent modulation of FBPase redox state, indicating that both factors are undoubtedly important to control the activity of this enzyme. In addition, it has been reported that Mg^{2+} protects FBPase from oxidative deactivation, due to the stabilizing role of the complex between the substrate FBP and Mg^{2+} [73].

In conclusion, we can assume that fluctuations in Mg^{2+} content occurring in the stroma might affect at multiple extents the activity and regulation of CrTK. Indeed, this metal ion is implicated (i) in the reconstitution of the fully active form, (ii) in the formation and stabilization of the holo-form, and finally (iii) in the modulation of the redox sensitivity of the enzyme. Further studies will be required on CrTK and other CBC enzymes to investigate the molecular mechanisms underlying the crosstalk between magnesium-induced and redox-induced light-dependent activation of photosynthetic carbon fixation.

Table 1. Data collection and refinement statistics for CrTK$_{apo}$ and CrTK$_{TPP/Mg}$ structure

	CrTK$_{TPP/Mg}$	CrTK$_{apo}$
Data collection		
Unit cell (Å)	201.49, 75.93, 103.76, 90.00, 109.99, 90.00	165.21, 74.31, 133.72, 90.00, 119.30, 90.00
Space group	C2	C2
Resolution range* (Å)	97.52 - 1.74 (1.82-1.74)	116.60 – 1.58 (1.64 – 1.58)
Unique reflections	114961	193102
Completeness* (%)	76.2 (64.6)	98.1 (97.9)
R$_{merge}$*	0.053 (0.240)	0.049 (0.567)
I/σ(I)	11.9 (1.7)	12.7 (1.9)
Multiplicity	2.1	3.3
Refinement		
Resolution range* (Å)	97.52- 1.74 (1.78-1.74)	116.61 – 1.58 (1.62 – 1.58)
Reflection used	109213 (6421)	180084 (13980)
R/R$_{free}$*	15.9/19.9 (21.3/25.4)	15.9/19.2 (30.4/31.8)
rmsd from ideality (Å, °)	0.02, 2.04	0.021, 1.97
N° atoms		
Non-hydrogen atoms	10815	11118
Protein atoms	10223	10219
Solvent molecules	538	841
Hetero atoms	54	58
B value (Å^2)		
Mean	17.7	26.2
Wilson plot	25.7	28.8
Protein atoms	17.5	26.1
Hetero atoms$^{\$}$	16.1	47.4
Solvent molecules	22.27	30.7
Ramachandran plot (%)		
Most favoured	97.7	97.1
Allowed	2.3	2.2
Disallowed	0.0	0.7

*The values in parenthesis refers to the last resolution shell.

$ The hetero atoms are 2 TPP molecules and 2 Mg^{2+} in CrTK$_{TPP/Mg}$ and 1EDO (ethylene glycol) molecule in CrTK$_{apo}$.

Acknowledgements

References

[1] G.A. Kochetov, O.N. Solovjeva, Structure and functioning mechanism of transketolase, Biochim. Biophys. Acta 1844 (2014) 1608-1618.

[2] G. Schenk, R.G. Duggleby, P.F. Nixon, Properties and functions of the thiamine diphosphate dependent enzyme transketolase, Int. J. Biochem. Cell Biol. 30 (1998) 1297-1318.

[3] E.R. van den Bergh, S.C. Baker, R.J. Raggers, P. Terpstra, E.C. Woudstra, L. Dijkhuizen, W.G. Meijer, Primary structure and phylogeny of the Calvin cycle enzymes transketolase and fructosebisphosphate aldolase of *Xanthobacter flavus,* J. Bacteriol. 178 (1996) 888-893.

[4] C.W. Hu, Y.L. Chang, S.J. Chen, L.L. Kuo-Huang, J.C. Liao, H.C. Huang, H.F. Juan, Revealing the functions of the transketolase enzyme isoforms in *Rhodopseudomonas palustris* using a systems biology approach, PLoS One 6 (2011) e28329.

[5] L. Michelet, M Zaffagnini, S. Morisse, F. Sparla, M.E. Pérez-Pérez, F. Francia, A. Danon, C.H. Marchand, S. Fermani, P. Trost, S.D. Lemaire, Redox regulation of the Calvin-Benson cycle: something old, something new, Front Plant Sci. 4 (2013) 470.

[6] Y. Lindqvist, G. Schneider, U. Ermler, M. Sundström, Three-dimensional structure of transketolase, a thiamine diphosphate dependent enzyme, at 2.5 A resolution, EMBO J. 11 (1992) 2373-2379.

[7] M. Nikkola, Y. Lindqvist, G. Schneider, Refined structure of transketolase from *Saccharomyces cerevisiae* at 2.0 Å resolution, J. Mol. Biol. 238 (1994) 387-404.

[8] P.C. Heinrich, H. Steffen, P. Janser, O. Wiss, Studies on the reconstitution of apotransketolase with thiamine pyrophosphate and analogs of the coenzyme, Eur. J. Biochem. 30 (1972) 533-541.

[9] S. Gerhardt, S. Echt, M. Busch, J. Freigang, G. Auerbach, G. Bader, W.F. Martin, A. Bacher, R. Huber, M. Fischer, Structure and properties of an engineered transketolase from maize, Plant Physiol. 132 (2003) 1941-1949.

[10] P. Schurmann, J.P. Jacquot, Plant thioredoxin systems revisited, Annu Rev Plant Physiol Plant Mol Biol. 51 (2000) 371-400.

[11] S. Morisse, L. Michelet, M. Bedhomme, C.H. Marchand, M. Calvaresi, P. Trost, S. Fermani, M. Zaffagnini, S.D. Lemaire, Thioredoxin-dependent redox regulation of chloroplastic phosphoglycerate kinase from *Chlamydomonas reinhardtii*, J Biol Chem. 289 (2014) 30012-30024.

[12] B.B. Buchanan, Y. Balmer, Redox regulation: a broadening horizon, Ann.Rev.Plant Biol 56 (2005) 187-220.

[13] S. Dai, R. Friemann, D.A. Glauser, F. Bourquin, W. Manieri, P. Schürmann, H. Eklund, Structural snapshots along the reaction pathway of ferredoxin-thioredoxin reductase, Nature 448 (2007) 92-96.

[14] S.D. Lemaire, L. Michelet, M. Zaffagnini, V. Massot, E. Issakidis-Bourguet, Thioredoxins in chloroplasts, Curr Genet. 51 (2007) 343-365.

[15] M. Teige, M. Melzer, K.H. Süss, Purification, properties and in situ localization of the amphibolic enzymes D-ribulose 5-phosphate 3-epimerase and transketolase from spinach chloroplasts, Eur J Biochem. 252 (1998) 237-244.

[16] Y. Balmer, A. Koller, G. del Val, W. Manieri, P. Schürmann, B.B. Buchanan, Proteomics gives insight into the regulatory function of chloroplast thioredoxins, Proc Natl Acad Sci U S A 100 (2003) 370-375.

[17] C. Marchand, P. Le Maréchal, Y. Meyer, M. Miginiac-Maslow, E. Issakidis-Bourguet, P. Decottignies, New targets of *Arabidopsis* thioredoxins revealed by proteomic analysis, Proteomics 4 (2004) 2696-2706.

[18] S.D. Lemaire, B. Guillon, P. Le Maréchal, E. Keryer, M. Miginiac-Maslow, P. Decottignies, New thioredoxin targets in the unicellular photosynthetic eukaryote *Chlamydomonas reinhardtii*,

29

Proc Natl Acad Sci U S A 101 (2004) 7475-7480.

[19] C. Marchand, P. Le Maréchal, Y. Meyer, P. Decottignies, Comparative proteomic approaches for the isolation of proteins interacting with thioredoxin, Proteomics 6 (2006) 6528-6537.

[20] A.G. Rocha, N. Mehlmer, S. Stael, A. Mair, N. Parvin, F. Chigri, M. Teige, U.C. Vothknecht, Phosphorylation of *Arabidopsis* transketolase at Ser428 provides a potential paradigm for the metabolic control of chloroplast carbon metabolism, Biochem. J. 458 (2014) 313-322.

[21] C.N. Pace, F. Vajdos, L. Fee, G. Grimsley, T. Gray, How to measure and predict the molar absorption coefficient of a protein, Protein Sci. 4 (1995) 2411-2423.

[22] F. Sparla, M. Zaffagnini, N. Wedel, R. Scheibe, P. Pupillo, P. Trost, Regulation of photosynthetic GAPDH dissected by mutants, Plant Physiol. 138 (2005) 2210-2219.

[23] M. Zaffagnini, S. Fermani, M. Calvaresi, R. Orrù, L. Iommarini, F. Sparla, G. Falini, A. Bottoni, P. Trost, Tuning Cysteine Reactivity and Sulfenic Acid Stability by Protein Microenvironment in Glyceraldehyde-3-Phosphate Dehydrogenases of *Arabidopsis thaliana*, Antioxid Redox Signal. 24 (2016) 502-517.

[25] C. Naula, V.P. Alibu, J.M. Brock, N.J. Veitch, R.J. Burchmore, M.P. Barrett, A new erythrose 4-phosphate dehydrogenase coupled assay for transketolase, J Biochem Biophys Methods 70 (2008) 1185-1187.

[25] S. Allenmark, Induced circular dichroism by chiral molecular interaction, Chirality 15 (2003) 409-422.

[26] D. Tedesco, C. Bertucci, Induced circular dichroism as a tool to investigate the binding of drugs to carrier proteins: classic approaches and new trends, J Pharm Biomed Anal. 113 (2015) 34-42.

[27] J. Jancarik, S.H. Kim, Sparse matrix sampling: a screening method for crystallization of proteins J. Appl. Cryst. 24 (1991) 409-411.

[28] W. Kabsch, XDS, Acta Cryst. D 66 (2010) 125-132.

[29] P. Evans, Scaling and assessment of data quality, Acta Cryst. D 62 (2006) 72-82.

[30] A. Vagin, A. Teplyakov, Molecular replacement with MOLREP, Acta Cryst. D 66 (2010) 22-25.

[31] A.T. Brünger, P.D. Adams, G.M. Clore, W.L. DeLano, P. Gros, R.W. Grosse-Kunstleve, J.S. Jiang, J. Kuszewski, M. Nilges, N.S. Pannu, R.J. Read, L.M. Rice, T. Simonson, G.L. Warren, Crystallography & NMR system: A new software suite for macromolecular structure determination, Acta Cryst. D 54 (1998) 905-921.

[32] G.N. Murshudov, A.A. Vagin, E.J. Dodson, Refinement of macromolecular structures by the maximum-likelihood method, Acta Cryst. D 53 (1997) 240-255.

[33] P. Emsley, K. Cowtan, Coot: model-building tools for molecular graphics, Acta Cryst. D 60 (2004) 2126-2132.

[34] E.H. Jung, T. Takeuchi, K. Nishino, Y. Itokawa, Studies on the nature of thiamine pyrophosphate binding and dependency on divalent cations of transketolase from human erythrocytes, Int.J.Biochem. 20 (1988) 1255-1259.

[35] G.A. Sprenger, U. Ulrich Schorken, G. Sprenger, H. Sahm, Transketolase A of *Escherichia coli* K12 Purification and properties of the enzyme from recombinant strains, Eur.J.Biochem. 230 (1995) 525-532.

[36] R.M. Egan, H.Z. Sable, Transketolase Kinetics. The slow reconstitution of the holoenzyme is due to rate-limiting dimerization of the subunits, JBC 256 (1981) 4877-4883.

[37] G.A. Kochetov, R.A. Usmanov, V.P. Merzlov, Thiamine pyrophosphate induced changes in the optical activity of baker's yeast transketolase, FEBS Lett. 9 (1970) 265-266.

31

[38] M.V. Kovina, I.A. Bykova, O.N.Solovjeva, L.E. Meshalkina, G.A. Kochetov, The origin of the absorption band induced through the interaction between apotransketolase and thiamin diphosphate, Biochem Biophys Res Commun. 294 (2002) 155-160.

[39] M.V. Kovina, A. de Kok, I.A. Sevostyanova, L.S. Khailova, N.V. Belkina, G.A. Kochetov, The molecular origin of the thiamin diphosphate-induced spectral bands of ThDP-dependent enzymes, PROTEINS: Structure, Function, and Bioinformatics 56 (2004) 338-345.

[40] C. Wikner, L. Meshalkina, U. Nilsson, M. Nikkola, Y. Lindqvist, M. Sundström, G. Schneider, Analysis of an invariant cofactor-protein interaction in thiamin diphosphate-dependent enzymes by site-directed mutagenesis. Glutamic acid 418 in transketolase is essential for catalysis, J Biol Chem. 269 (1994) 32144-32150.

[41] M. Zaffagnini, M. Bedhomme, H. Groni, C.H. Marchand, C. Puppo, B. Gontero, C. Cassier-Chauvat, P. Decottignies, S.D. Lemaire, Glutathionylation in the photosynthetic model organism *Chlamydomonas reinhardtii*: a proteomic survey, Mol Cell Proteomics 11 (2012) M111.014142.

[42] D. Kern, G. Kern, H. Neef, K. Tittmann, M. Killenberg-Jabs, C. Wikner, G. Schneider, G. Hübner, How thiamine diphosphate is activated in Enzymes, Science 275 (1997) 67-70.

[43] L. Nauton, V. Hélaine, V. Théry, L. Hecquet, Insights into the Thiamine Diphosphate Enzyme Activation Mechanism: Computational Model for Transketolase Using a Quantum Mechanical/Molecular Mechanical Method, Biochemistry 55 (2016) 2144-2152.

[44] J. Pletcher, M. Sax, Crystal and molecular structure of thiamine pyrophosphate hydrochloride J Am Chem Soc 94 (1972) 3998-4005.

[45] E.B. Getz, M. Xiao, T. Chakrabarty, R. Cooke, P.R. Selvin, A comparison between the sulfhydryl reductants tris(2-carboxyethyl)phosphine and dithiothreitol for use in protein biochemistry, Anal. Biochem. 273 (1999) 73-80.

[46] G.K. Kochetov, P.P. Philippov, The function of calcium-cofactor of transketolase from baker's yeast, FEBS Letters 6 (1970) 49-51.

[47] D.C. Lin, P.S. Nobel, Control of photosynthesis by Mg^{2+}, Arch. Biochem. Biophys. 145 (1971) 622-632.

[48] S. Ishijima, A. Uchibori, H. Takagi, R. Maki, M. Ohnishi, Light-induced increase in free Mg^{2+} concentration in spinach chloroplasts: Measurement of free Mg^{2+} by using a fluorescent probe and necessity of stromal alkalinization, Arch. Biochem. Biophys. 412 (2003) 126-132.

[49] G. Schneider, Y. Lindqvist, Enzymatic thiamine catalysis: mechanistic implication from the three-dimensional structure of transketolase, Bioorg. Chem. 21 (1993) 109-117.

[50] A. Schellenberger, The amino group and steric factors in thiamin catalysis, Annals N.Y. Acad. of Sciences 378 (1982) 51-62.

[51] R. Friedemann, C. Breitkopf, Theoretical studies on thiamin-substrate adducts, Bioorg. Chem. 22 (1994) 119-127.

[52] A. Schellenberger, Sixty years of thiamin diphosphate biochemistry, Biochim. Biophys. Acta 1385 (1998) 177-186.

[53] L.E. Meshalkina, G.A. Kochetov, The functional identity of the active centers of transketolase, Biochim. Biophys. Acta 571 (1979) 218-223.

[54] G.A. Kochetov, Structure of the active center of transketolase, Annals N.Y. Acad. of Sciences 378 (1982) 306-311.

[55] G. Schneider, Y. Lindqvist, Crystallography and mutagenesis of transketolase: mechanisticimplications for enzymatic thiamin catalysis, Biochim. Biophys. Acta 1385 (1998) 387-398.

33

[56] M. Sundstrom, Y. Lindqvist, G. Schneider, Three-dimensional structure of apotransketolase. Flexible loops at the active site enable cofactor binding, FEBS Lett. 313 (1992) 229-231.

[57] A.M. El-Badry, Hexosediphosphatase from spinach chloroplasts purification, crystallization and some properties, Biochim. Biophys. Acta 333 (1974) 366-377.

[58] K. Werdan, H.W. Heldt, M. Milovancev, The role of pH in the regulation of carbon fixation in the chloroplast stroma. Studies on CO_2 fixation in the light and dark, Biochim. Biophys. Acta 396 (1975) 276-292.

[59] Y. Balmer, A. Koller, G.D. Val, P. Schürmann, B.B. Buchanan, Proteomics uncovers proteins interacting electrostatically with thioredoxin in chloroplasts, Photosynth Res. 79 (2004) 275-280.

[60] A.R.J. Portis, H.W. Heldt, Light-dependent changes of the Mg^{2+} concentration in the stroma in relation to the Mg^{2+} dependency of CO_2 fixation in intact chloroplasts, Biochim Biophys Acta. 449 (1976) 434-446.

[61] O. Shaul, Magnesium transport and function in plants: the tip of the iceberg, BioMetals 15 (2002) 309-323.

[62] C. Hermans, S.J. Conn, J. Chen, Q. Xiao, N. Verbruggen, An update on magnesium homeostasis mechanisms in plants, Metallomics 5 (2013) 1170-1183.

[63] W.H. Heldt, K. Werdan, M. Milovancev, G. Geller, Alkalization of the chloroplast stroma caused by light-dependent proton flux into the thylakoid space, Biochim Biophys Acta 314 (1973) 224-241.

[64] G. Hind, H.Y. Nakatani, S. Izawa, Light-dependent redistribution of ions in suspensions of chloroplast thylakoid membranes, Proc Natl Acad Sci U S A 71 (1974) 1484-1488.

[65] A.N. Tikhonov, pH-dependent regulation of electron transport and ATP synthesis in chloroplasts, Photosynth Res. 116 (2013) 511-534.

[66] G.H. Krause, Changes in chlorophyll fluorescence in relation to light-dependent cation transfer across thylakoid membranes, Biochim Biophys Acta 333 (1974) 301-313.

[67] G. Zimmermann, G.J. Kelly, E. Latzko, Efficient purification and molecular properties of spinach chloroplast fructose 1,6-bisphosphatase, Eur J Biochem. 70 (1976) 361-367.

[68] A.N. Nishizawa, B.B. Buchanan, Enzyme regulation in C4 photosynthesis. Purification and properties of thioredoxin-linked fructose bisphosphatase and sedoheptulose bisphosphatase from corn leaves, J Biol Chem. 256 (1981) 6119-6126.

[69] R. Minot, J.C. Meunier, J. Buc, J. Ricard, The role of pH and magnesium concentration in the light activation of chloroplastic fructose bisphosphatase, FEBS Letters 142 (1982) 118-120.

[70] I.E. Woodrow, D.J. Murphy, E. Latzko, Regulation of stromal sedoheptulose 1,7-bisphosphatase activity by pH and Mg^{2+} concentration, J Biol Chem. 259 (1984) 3791-3795.

[71] F. Cadet, J.C. Meunier, pH and kinetic studies of chloroplast sedoheptulose-1,7-bisphosphatase from spinach (*Spinacia oleracea*), Biochem J. 253 (1988) 249-254.

[72] D.D. Gütle, T. Roret, S.J. Müller, J. Couturier, S.D. Lemaire, A. Hecker, T. Dhalleine, B.B. Buchanan, R. Reski, O. Einsle, J.P. Jacquot, Chloroplast FBPase and SBPase are thioredoxin-linked enzymes with similar architecture but different evolutionary histories, Proc Natl Acad Sci U S A 113 (2016) 6779-6784.

[73] P. Schürmann, B.B. Buchanan, The ferredoxin/thioredoxin system of oxygenic photosynthesis Antioxid Redox Signal. 10 (2008) 1235-1274.

[74] A.C. Wallace, R.A. Laskowski, J.M. Thornton, LIGPLOT: a program to generate schematic diagrams of protein-ligand interactions, Protein Eng. 8 (1996) 127-134.

[75] O. Emanuelsson, H. Nielsen , G. von Heijne, ChloroP, A neural network-based method for

predicting chloroplast transit peptides and their cleavage sites, Protein Sci. 8 (1999) 978-84.

[76] M. Tardif, A. Atteia, M. Specht, G. Cogne, N. Rolland, S. Brugière, M. Hippler, M. Ferro, C. Bruley, G. Peltier, O. Vallon, L. Cournac, PredAlgo: A New Subcellular Localization Prediction Tool Dedicated to Green Algae, Mol. Biol. Evol. 29 (2012) 3625-3639.

[77] F. Sievers, A. Wilm, D. Dineen, T.J. Gibson, K. Karplus, W. Li, R. Lopez, H. McWilliam, M. Remmert, J. Söding, J.D. Thompson, D.G. Higgngs, Fast, scalable generation of high-quality protein multiple sequence alignments using Clustal Omega, Mol. Syst. Biol. 7 (2011) 539.

[78] X. Robert, P. Gouet, Deciphering key features in protein structures with the new ENDscript server, Nucleic Acids Res. 42 (2014) 320-324.